Research paper

Heterogeneous occurrence of evergreen broad-leaved forests in East Asia: Evidence from plant fossils

Jiagang Zhao [a, b], Shufeng Li [a], Jian Huang [a], Wenna Ding [a, c], Mengxiao Wu [a, d], Tao Su [a, e], Alexander Farnsworth [f, g], Paul J. Valdes [f], Linlin Chen [f], Yaowu Xing [a, *], Zhekun Zhou [a, **]

[a] CAS Key Laboratory of Tropical Forest Ecology, Xishuangbanna Tropical Botanical Garden, Chinese Academy of Sciences, Mengla 666303, China
[b] University of Chinese Academy of Sciences, Beijing 100049, China
[c] Swiss Federal Institute for Forest, Snow and Landscape Research WSL, 8903 Birmensdorf, Switzerland
[d] Senckenberg Natural History Collections Dresden, Königsbrücker Landstraße 159, 01109 Dresden, Germany
[e] State Key Laboratory of Oil and Gas Reservoir Geology and Exploitation & Institute of Sedimentary Geology, Chengdu University of Technology, Chengdu 610059, China
[f] School of Geographical Sciences, University of Bristol, Bristol BS8 1SS, UK
[g] State Key Laboratory of Tibetan Plateau Earth System, Environment and Resources (TPESER), Institute of Tibetan Plateau Research, Chinese Academy of Sciences, Beijing 100101, China

ARTICLE INFO

ABSTRACT

Evergreen broad-leaved forests (EBLFs) are widely distributed in East Asia and play a vital role in ecosystem stability. The occurrence of these forests in East Asia has been a subject of debate across various disciplines. In this study, we explored the occurrence of East Asian EBLFs from a paleobotanical perspective. By collecting plant fossils from four regions in East Asia, we have established the evolutionary history of EBLFs. Through floral similarity analysis and paleoclimatic reconstruction, we have revealed a diverse spatio-temporal pattern for the occurrence of EBLFs in East Asia. The earliest occurrence of EBLFs in southern China can be traced back to the middle Eocene, followed by southwestern China during the late Eocene—early Oligocene. Subsequently, EBLFs emerged in Japan during the early Oligocene and eventually appeared in central-eastern China around the Miocene. Paleoclimate simulation results suggest that the precipitation of wettest quarter (PWetQ, mm) exceeding 600 mm is crucial for the occurrence of EBLFs. Furthermore, the heterogeneous occurrence of EBLFs in East Asia is closely associated with the evolution of the Asian Monsoon. This study provides new insights into the occurrence of EBLFs in East Asia.

1. Introduction

Evergreen broad-leaved forests (EBLFs) are a forest community type consisting of evergreen dicotyledonous plants with high endemism and rich biodiversity, dominated by families such as Fagaceae, Lauraceae, Magnoliaceae and Theaceae (Wu, 1995; Song, 2013; Tang, 2015; Song and Da, 2016; Fig. 1). These forests occupy large areas in East Asia, especially in southern China, southern Japan, and southernmost Korea (Song and Da, 2016; Fig. 1).

Compared to other latitudinal bands worldwide, particularly those with semi-arid or arid desert conditions, EBLFs predominantly occur under monsoon climates and exhibit significantly higher productivity in East Aisa (Tang, 2015; Song and Da, 2016). They hold significant importance as terrestrial ecosystems, substantially enhancing global forest ecosystem services, providing various biological resources, and promoting sustainable social development (Piao et al., 2009; Pan et al., 2011; Fang et al., 2014; Tang, 2015). Therefore, understanding the historical dynamics of EBLFs and their underlying drivers is crucial for conserving their diversity in East Asia. However, the origin and evolution of EBLFs remains controversial across different disciplines.

The historical dynamics of EBLFs have been reconstructed using molecular approaches. For instance, molecular dating of Fagaceae
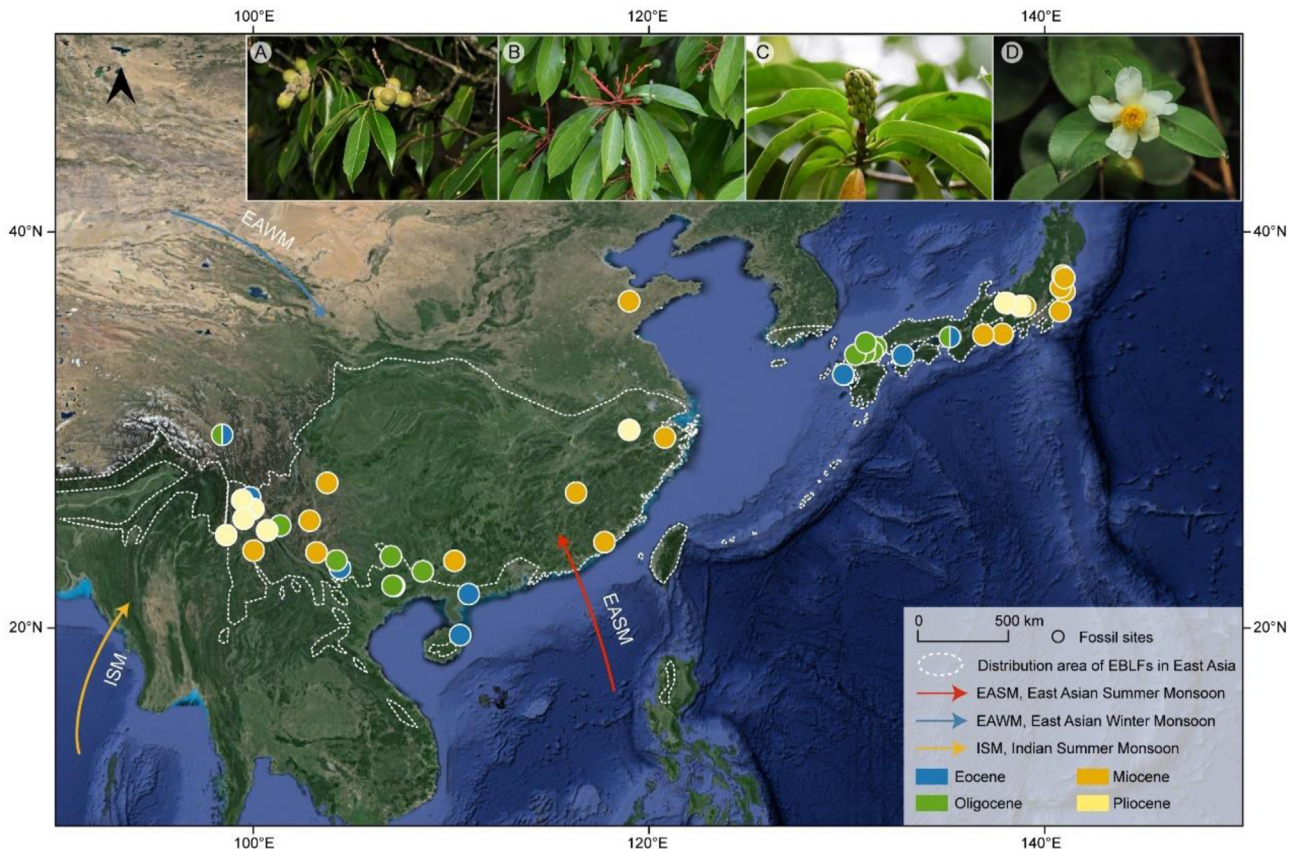
Fig. 1. The distribution range of modern EBLFs and fossil sites in East Asia. White dashed lines delineate the distribution range of modern EBLFs (Illustrated by Jian Huang). The dots represent fossil sites with various colors in different geological ages. Pictures of dominant families for EBLFs: (A) Fagaceae, (B) Lauraceae, (C) Magnoliaceae, (D) Theaceae (Photographs from Jian Huang).

(Xiang et al., 2014; Xing et al., 2014; Hipp et al., 2020; Hai et al., 2022), Theaceae (Yu et al., 2017; Rao et al., 2018), Lauraceae (Li et al., 2011; Huang et al., 2016a; Xiao et al., 2022; Qin et al., 2023), and Magnoliaceae (Azuma et al., 2001; Nie et al., 2008; Dong et al., 2021) have all indicated that EBLFs emerged in the Eocene. Other key groups, e.g., *Dendrobium* (Orchidaceae), *Quercus* Section *Cyclobalanopsis* (Fagaceae) and *Mahonia* (Berberidaceae), have suggested that EBLFs may have been established in mainland Asia during the early Oligocene (Xiang et al., 2016; Deng et al., 2018; Chen et al., 2020). Meta-analysis of 72 generic-level characteristic lineages has also demonstrated that the origin of EBLFs can be traced back to the early Oligocene (Zhang et al., 2024). Several synthetic studies using many lineages have proposed that the East Asian flora (EAF) might be relatively young, with most of its clades originating since the Miocene (Chen et al., 2018; Lu et al., 2018). Furthermore, many studies have demonstrated that a rapid radiation occurred in East Asia during the Miocene (Yu et al., 2017; Deng et al., 2018; Chen et al., 2020; Yan et al., 2021; Hai et al., 2022; Zhang et al., 2022).

Plant fossil records provide more direct and reliable evidence for the origin and evolution of EBLFs. High-quality geochronological studies have called for re-examining the emergence of these forests. The previously presumed Miocene strata (WGCPC, 1978; BGMRYP (Bureau of Geology and Mineral Resources of Yunnan Province), 1990, BGMRYP (Bureau of Geology and Mineral Resources of Yunnan Province), 1996; Xu et al., 2008; Li et al., 2015; Huang et al., 2016b, 2017, 2018) for many fossil floras in southwestern China has now been revised to be late Eocene/early Oligocene in age (Gourbet et al., 2017; Linnemann et al., 2018; Su

et al., 2019; Tian et al., 2021). Evergreen representatives, including Fagaceae, Lauraceae and Fabaceae, are main components in these floras (Huang, 2017; Su et al., 2019; Deng et al., 2020; Tian et al., 2021; Wu et al., 2022b). The revised geological ages and components of fossil floras indicate that the temporal occurrence of EBLFs may have been advanced to the late Eocene—early Oligocene in southwestern China. Likewise, plant fossil records in southern China with high diversity of evergreen elements demonstrate that EBLFs emerged in this region at least from the middle Eocene (Spicer et al., 2014, 2016; Aleksandrova et al., 2015; Herman et al., 2017; Averianov et al., 2017). The discrepancy between molecular and paleobotanical evidence suggests a complex evolutionary history of EBLFs in East Asia, and a comprehensive understanding of this issue requires deep exploration.

Long-term climate changes have influenced the development of specific biomes over time. The Asian monsoon has played a critical role in the formation of EBLFs by bringing a humid climate that has facilitated their historical assembly (Song and Da, 2016; Yu et al., 2017; Li et al., 2021a). The relationship between the evolution of the Asian monsoon and the emergence of EBLFs remains unclear, probably because the timing of the onset of the Asian monsoon is controversial. Some researchers have suggested that the Asian monsoon originated around the Oligocene—Miocene boundary (Sun and Wang, 2005; Guo et al., 2008; Lin et al., 2015), whereas others argue that it emerged as early as the Eocene (Wang et al., 2013; Quan et al., 2014; Licht et al., 2014; Li et al., 2022) or even the Paleocene (Spicer et al., 2016; Spicer, 2017). A recent review that integrated proxy data and modeling evidence proposed a two-stage northward expansion process for the Asian monsoon (Wu et al.,

2022a). This study suggests that the dynamics of EBLFs may undergo multiple stages, providing us an opportunity to deeply explore how climate variations influence the spatial and temporal patterns of vegetation.

In this study, we use paleobotanical evidence to identify when and where EBLFs have occurred in East Asia. Based on a large dataset of the Cenozoic macrofossil records in East Asia, we reconstructed the fossil history of EBLFs' dominant genera, determined the most similar extant vegetation, calculated the paleoclimate for each fossil assemblage, as well as simulated the paleoclimate during the Cenozoic. We further explored the relationship between the historical dynamics of EBLFs and climate evolution. Our results demonstrate that occurrence of EBLFs in East Asia is heterogeneous, which is closely linked with the evolution of the Asian Monsoon.

2. Materials and methods

2.1. Paleobotanical data

We compiled a dataset of Cenozoic paleobotanical records from East Asia, focusing on macrofossils such as leaves, seeds, fruits, and wood to minimize biases caused by potentially long-distance transport of pollen grains. We excluded fossil assemblages with fewer than ten taxa, resulting in a selection of 50 assemblages from 47 fossil floras (Fig. 1 and Table 1). Geographic locations and climatic conditions (Song, 2013; Song and Da, 2016) were used to classify the fossil assemblages into four regions: southwestern China (including southeastern Xizang and Yunnan), southern China (including Guangxi, Guangdong, and Hainan), central-eastern China (including Jiangxi, Shandong, Zhejiang, and Fujian), and Japan (including central and southwestern regions) (Fig. 1 and Table 1). More detailed information on each fossil assemblage is provided in Table S1. Moreover, we identified the dominant genera among all fossil taxa based on their roles in modern EBLFs (Table S2) and calculated the probability density distribution of these genera appearing in different geological periods within each region.

2.2. Flora similarity analysis

We used the Phytogeographic Reference Region Assessment (PRRA) approach to determine the most similar extant forest vegetation for each fossil assemblage (Kunzmann et al., 2022). Prior to analysis, the fossil taxa were assigned to their nearest living relatives (NLRs). The NLRs were primarily retrieved from primary literature; if NLRs were not mentioned in the literature, we referred to the PALAEOFLORA database (www.palaeoflora.de). Distribution data for NLRs were obtained from the Global Biodiversity Information Facility database (GBIF, www.gbif.org) and processed using the methods described by Palazzesi et al. (2014) and Kunzmann et al. (2022). By calculating the number of overlapping taxa between NLRs and modern global vegetation data to assess the degree of similarity in grids for each fossil assemblage. Then we calculated the mean similarity across the four regions over different geological periods. Given the high similarity between them, the modern vegetation type of high similarity grids can be considered the same as the vegetation type of fossil assemblages. PRRA analysis was conducted in R with a 2° grid resolution, following the procedure outlined by Kunzmann et al. (2022).

2.3. Quantitative reconstruction of the paleoclimate

We used Joint Probability Density Functions (JPDFs) to reconstruct the paleoclimate of each fossil assemblage (Willard et al.,

2019). This method assumed that the ecological tolerance of plant fossils is comparable to their NLRs (Utescher et al., 2014). Thus, taxa that exhibit significant changes in their distribution over geological time, such as relict plants (e.g., *Metasequoia*, *Ginkgo*, *Glyptostrobus*, and *Cyclocarya*), should not be considered for reconstruction process. Several widespread fossil taxa were also excluded in the reconstruction process, as they would have been of limited value for determination of climatic conditions, such as Pinaceae, Poaceae, and Polygonaceae.

Similar to the PRRA approach described in section 2.2, the JPDFs also depend on the climatic distribution of NLRs. Raw data derived from GBIF were cleaned by removing repeated coordinates, erroneous coordinates, cultivation sites, wherever possible, and gridded (keep only one occurrence in 5′ × 5′ area) distribution data using the "gridSample" function of the R package "dismo". Modern climatic data were obtained from CHELSA (Climatologies at high resolution for the earth's land surface areas) climate database (chelsa-climate.org, Karger et al., 2017). The most likely climatic conditions of each fossil assemblage were then calculated by cross-plotting the probability density of each taxon (Willard et al., 2019; West et al., 2020).

In total, six climatic variables were calculated using this quantitative method, namely mean annual temperature (MAT, °C), mean temperature of the warmest month (MTWM, °C), mean temperature of the coldest month (MTCM, °C), mean annual precipitation (MAP, mm), precipitation of the wettest quarter (PWetQ, mm), and precipitation of the driest quarter (PDryQ, mm).

2.4. Numerical simulations of the paleoclimate

We used the Hadley Centre Coupled Model (v.3 low resolution; HadCM3BL) from the University of Bristol in the UK, to simulate paleoclimatic conditions (Valdes et al., 2021; Fenton et al., 2023). The HadCM3BL is a fully coupled atmosphere-ocean general circulation model with a low resolution of 3.75° longitude × 2.5° latitude, 19 vertical atmosphere levels and 20 ocean depth levels (Valdes et al., 2017). The land surface scheme used the Met Office Surface Exchange Scheme (MOSES 2.1) and the vegetation predicted used a dynamic vegetation and terrestrial carbon cycle scheme, TRIFFID (Top-down Representation of Interactive Foliage and Flora Including Dynamics) (Cox, 2001; Valdes et al., 2017).

The boundary conditions were constrained as follows: the solar constant of each period was increased linearly to the modern value, and the earth orbit parameters were set to present conditions. The land-sea boundary, topography, and ice sheets were derived from the Scotese (2021). CO_2 concentrations were set according to the values presented in Foster et al. (2017) (Table S3). Based on these boundary conditions, the paleoclimate of different periods during the Cenozoic was simulated. Each snap shot experiment was run for 1000 model years and reached an equilibrium state in both the surface and deep ocean, with no energy imbalance at the top of the atmosphere (Valdes et al., 2021). The mean of the last 100 model years was regarded as the simulated outputs in our research. The raw output climate data were interpolated to high-resolution data (5′) to facilitate visualization in figures and comparison with fossil data using the "resample" function from the "terra" package in R. Numerical simulations offer a thorough representation of climatic patterns, providing valuable insights to supplement the limited temporal and spatial coverage of fossil records. As such, the simulated results were compared to reconstructions based on fossil records.

To evaluate the performance of the model, we compared the simulated modern output (Fig. 5I) with a very high resolution (30 arc sec, ~1 km) observed data in 1981~2010 from CHELSA climate database (chelsa-climate.org, Karger et al., 2017; Fig. S1). The

Table 1
Information on fossil assemblages.

No.	Fossil assemblages	Region	Location	Age
1	Changchang	southern China	19.64°N, 110.45°E	middle Eocene
2	Shangsi		22.12°N, 107.13°E	middle Eocene
3	Nanning		22.86°N, 108.57°E	Eocene
4	Nanning		22.86°N, 108.57°E	late Oligocene
5	Maoming		21.71°N, 110.89°E	middle Eocene
6	Maoming		21.71°N, 110.89°E	late Eocene
7	Baise		23.62°N, 106.96°E	early Oligocene
8	Ningming		22.13°N, 107.04°E	Oligocene
9	Guiping		23.39°N, 110.17°E	Miocene
10	Markam	southwestern China	29.75°N, 98.43°E	late Eocene
11	Markam		29.75°N, 98.43°E	early Oligocene
12	Maguan		23.02°N, 104.38°E	late Eocene
13	Jianchuan		26.60°N, 99.84°E	late Eocene
14	Wenshan		23.40°N, 104.21°E	early Oligocene
15	Lühe		25.17°N, 101.37°E	early Oligocene
16	Kaiyuan		23.81°N, 103.20°E	late Miocene
17	Zhaotong		27.33°N, 103.74°E	late Miocene
18	Lincang		23.90°N, 100.02°E	late Miocene
19	Xianfeng		25.42°N, 102.85°E	late Miocene
20	Tengchong		24.69°N, 98.63°E	Pliocene
21	Eryuan		26.02°N, 100.00°E	Pliocene
22	Lanping		26.46°N, 99.44°E	Pliocene
23	Yuanmou		24.92°N, 100.70°E	Pliocene
24	Yongping		25.51°N, 99.52°E	Pliocene
25	Shanwang	central-eastern China	36.50°N, 119.00°E	middle Miocene
26	Tiantai		29.62°N, 120.80°E	middle Miocene
27	Guangchang		26.83°N, 116.32°E	middle Miocene
28	Zhangpu		24.33°N, 117.75°E	middle Miocene
29	Yuyao		30.00°N, 119.00°E	Pliocene
30	Ube	Japan	34.00°N, 131.00°E	late Eocene
31	Takashima		32.80°N, 129.82°E	late Eocene
32	Myojin		33.77°N, 132.83°E	late Eocene
33	Kobe		34.69°N, 135.20°E	late Eocene—early Oligocene
34	Northwestern Kobe		33.90°N, 130.80°E	early Oligocene
35	Ouchiyama-kami		34.18°N, 131.48°E	Oligocene
36	Shimokatakura		33.97°N, 131.29°E	Oligocene
37	Shimonoseki		33.90°N, 130.90°E	early Oligocene
38	Tsuyazaki		33.80°N, 130.43°E	early Oligocene
39	Noda		34.40°N, 130.95°E	late Oligocene
40	Shichiku		36.00°N, 140.77°E	early Miocene
41	Kunugidaira		37.00°N, 141.00°E	early Miocene
42	Shiote		37.80°N, 140.90°E	early Miocene
43	Nakayama		37.20°N, 140.80°E	early Miocene
44	Ouchi		37.68°N, 140.99°E	early Miocene
45	Ieda Group		34.85°N, 137.87°E	middle Miocene
46	Northwestren Kwanto District		36.25°N, 139.00°E	late Miocene
47	Ogawa		36.40°N, 138.10°E	late Miocene
48	Seto Group		34.80°N, 136.90°E	late Miocene
49	Kabutoiwa		36.25°N, 138.75°E	Pliocene
50	Ohoka		36.42°N, 138.00°E	Pliocene

simulated modern output was generally consistent with the observations. However, there was a slight discrepancy in northern China, which is likely due to the resolution difference between the model and observations. In addition, through a detailed comparison with other models available in Coupled Model Intercomparison Project Phase 5 (CMIP5), it has been shown that the HadCM3BL performed relatively well (Valdes et al., 2017). Therefore, this model can be used to capture the broad features of the climate, and provide important clues for understanding Cenozoic climate change.

3. Results

3.1. The fossil history of dominant genera for East Asian EBLFs

Probability density distribution analysis indicate that the timing of appearance for EBLFs' dominant genera varied across four regions (Fig. 2). In southern China, dominant genera appeared as early as the Paleocene—early Eocene and peaked in the middle

Eocene, followed by a continuous decline (Fig. 2A). While they firstly appeared in southwestern China during the middle Eocene and peaked in the late Eocene—early Oligocene, after that dominant genera declined rapidly in the late Oligocene—early Miocene before rebounding in the late Miocene (Fig. 2B). In Japan, dominant genera appeared in the middle Eocene, peaked in the early Oligocene, and continued to decrease with a sub-peak in the late Miocene—Pliocene (Fig. 2C). In central-eastern China, the peak of dominant genera occurred around the middle Miocene. Afterwards, two consecutive small peaks occurred in the late Miocene and Pliocene (Fig. 2D).

3.2. Similarity analysis results for fossil assemblages

PRRA results showed that high similarity areas (the colored red grid boxes with high co-occurrence values) for the four examined regions differ, but each region nearly matches its modern location (Fig. 3). In southern China, the concentration of high similarity
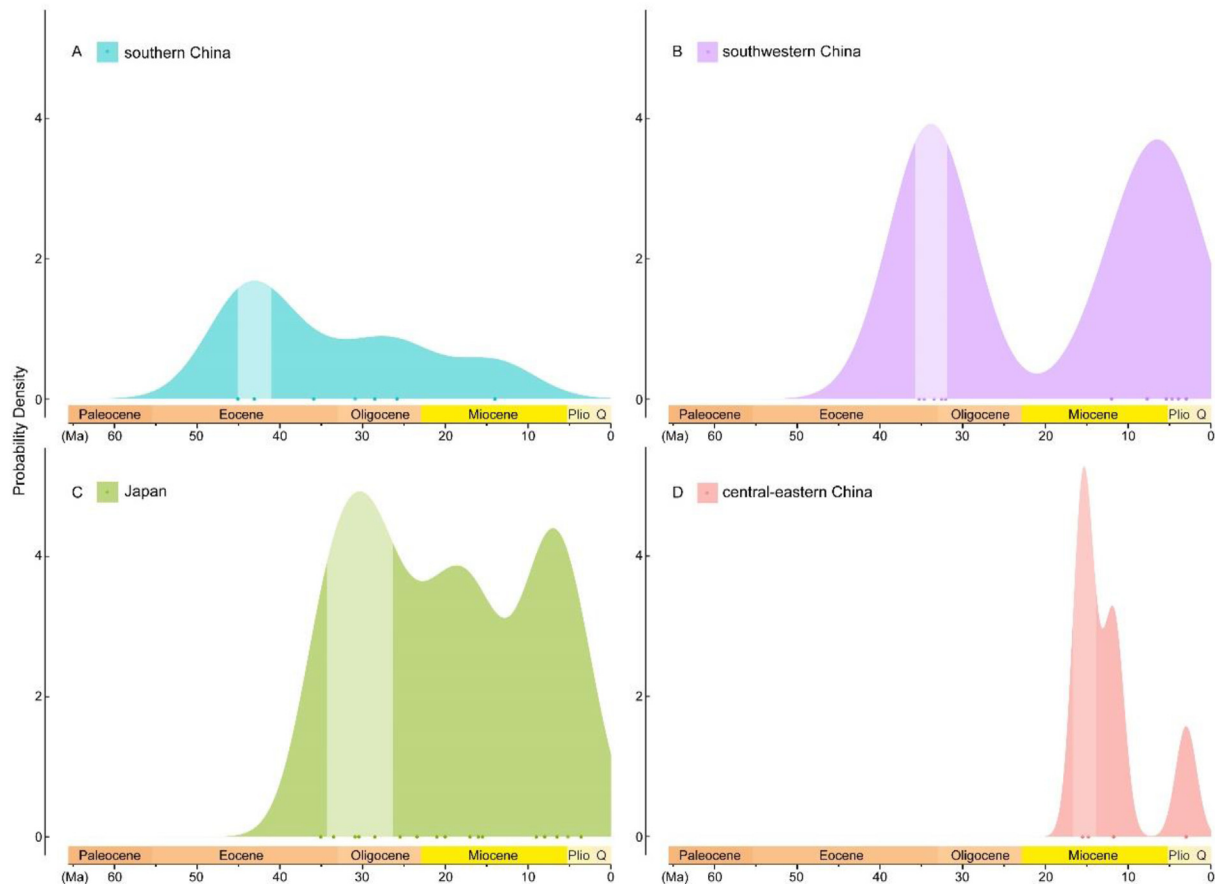
Fig. 2. The probability density distribution of dominant genera that appeared in different geological time for four regions. The shaded area represents the peak period of appearance for dominant genera.

areas between fossil assemblages and modern vegetation generally increased from the middle Eocene to Miocene (Fig. 3A). During the middle Eocene, the high similarity area was widely distributed in southern China (Fig. 3A1), but then gradually contracted to the northern part of the Indochina Peninsula (Figs. 3A4 and S10). In southwestern China, high similarity areas have changed slightly and are mainly distributed in southeastern Xizang, Yunnan and Sichuan (Fig. 3B). In comparison to other periods, the similarity area was more concentrated in northwestern Yunnan during the Pliocene (Fig. 3B4). In the early Oligocene, the high similarity area of the Markam assemblage was not only distributed in southwestern China, but also in southwestern Japan and western Europe (Fig. S12). In Japan, high similarity areas have undergone significant changes. These areas were originally located in southeastern China during the late Eocene (Fig. 3C1). However, they shifted to southwestern Japan from the Oligocene (Fig. 3C2—C4). In central-eastern China, high similarity areas were widely distributed in eastern China, with the highest concentration in Jiangxi and Anhui (Fig. 3D). The similarity areas of middle Miocene Zhangpu assemblage were mainly distributed in Southeast Asia (Fig. S29).

3.3. Quantitative paleoclimate reconstruction from plant fossils

Table S4 shows the paleoclimatic data using the Joint Probability Density Functions (JPDFs) for each plant fossil assemblage of East Asia, including six climate variables, i.e., MAT, MTCM, MTWM, MAP, PWetQ, PDryQ. Of these, MAT, MTCM and MAP were employed to assess whether a fossil assemblage fulfills the climatic criteria of EBLFs in East Asia.

The EBLFs on the East Asian occurred under monsoon climate, with hot, moist summers and fairly cold winters. Our reconstructed paleoclimates show that EBLFs in each regions exhibited distinct climatic conditions. EBLFs cannot be established if dominant taxa are unable to tolerate climatic conditions of each region (the climatic conditions shown by dashed lines in Fig. 4). The key limiting factor for the establishment of EBLFs was MTCM, with values needing to exceed the minimum threshold to prevent damage from freezing temperatures.

In southern China, the emergence of EBLFs requires the highest temperature and precipitation. Our reconstruction indicated that MAT ranged from 19 °C to 21 °C, MTCM from 9 °C to 12 °C, and MAP from 1500 mm to 2200 mm (shown by dashed line in Fig. 4A). Most of the reconstructed paleoclimates align with these climatic conditions. However, the reconstructed MAT of the late Eocene Maoming assemblage was below the minimum limit, ranging from 12.95 °C to 17.35 °C (Fig. 4A1, No. 5). Conversely, the reconstructed MTCM of the Miocene Guiping assemblage exceeded the maximum limit, ranging from 13.15 °C to 15.95 °C (Fig. 4A2, No.9).

The climatic conditions conducive to the emergence of EBLFs in the southwestern China were relatively lower, with MAT ranging from 10 °C to 20 °C, MTCM from 4 °C to 12 °C, and MAP from 800 mm to 1500 mm (shown by dashed line in Fig. 4B). The reconstructed MAT and MAP of all fossil assemblages in this region satisfy these criteria, except for the early Oligocene Markam assemblage, where the reconstructed MTCM falls below the minimum threshold, ranging from −4.15 °C to 3.95 °C (Fig. 4B2, No.11).

EBLFs occurred in Japan under climatic conditions that required lower temperatures and higher precipitation. The MAT ranged from
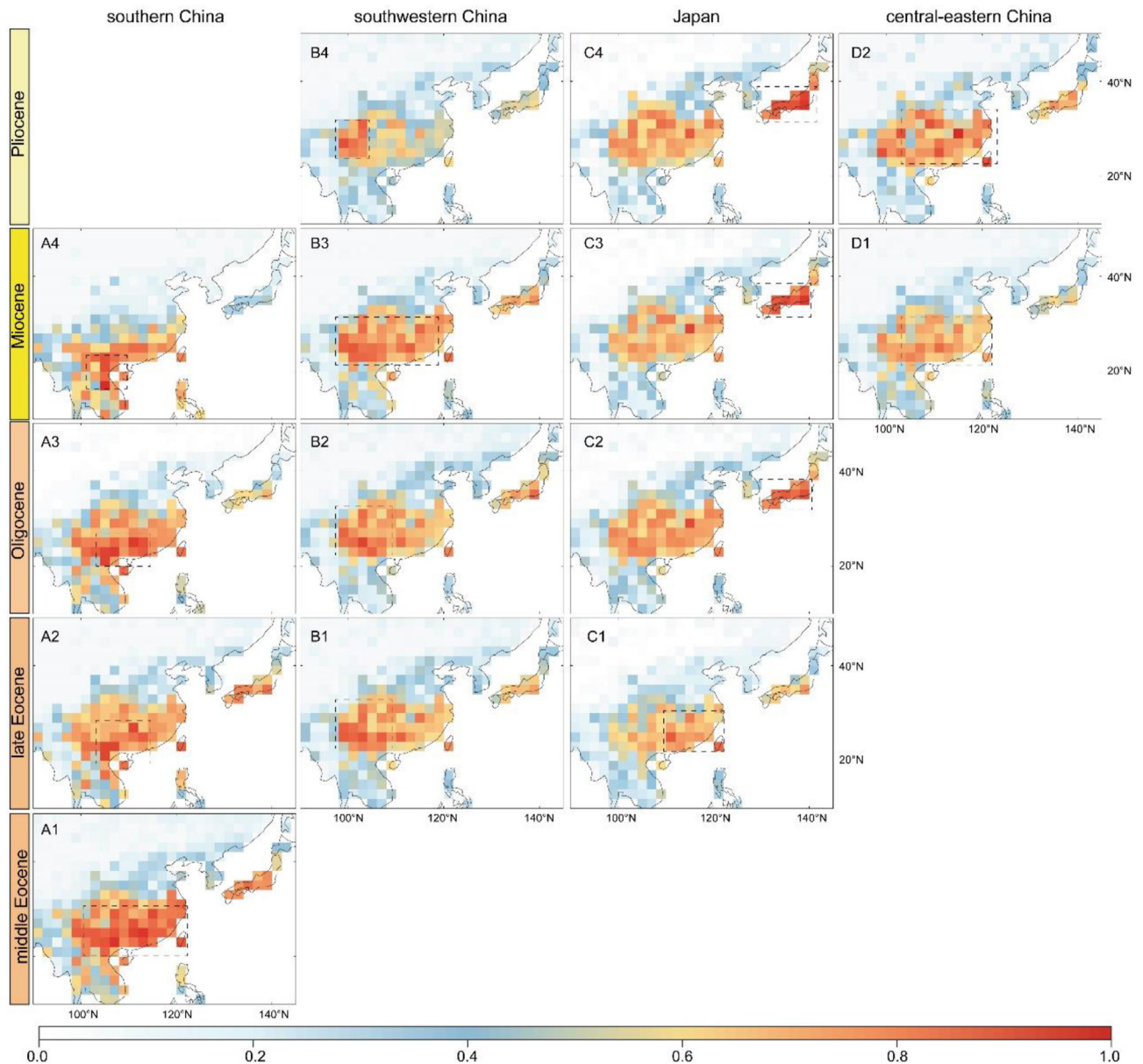
Fig. 3. Mean similarity between the fossil assemblages and modern vegetation for four regions in different geological periods. The black dashed boxes indicate the high similarity areas.

13 °C to 18 °C, MTCM from 0.9 °C to 10 °C, and MAP from 1200 mm to 2500 mm (shown by dashed line in Fig. 4C). The reconstructed MTCM and MAP of all fossil assemblages in this region meet these conditions, except the reconstructed MAT of the early Miocene Shichiku assemblage, which is lower than the minimum limit, ranging from 9.85 °C to 12.85 °C (Fig. 4C1, No.40).

Compared with other regions, the climatic conditions for the emergence of EBLFs in central-eastern China were relatively moderate, with MAT ranging from 15 °C to 18 °C, MTCM from 2 °C to 10 °C, and MAP from 1000 mm to 2000 mm (shown by dashed line in Fig. 4D). The reconstructed climates of most fossil assemblages in this region align with these conditions, except for the middle Miocene Zhangpu assemblage, which exceeds the maximum standard, with reconstructed MAT and MTCM ranging from 20.55 °C to 24.15 °C and 16.65 °C—21.95 °C, respectively (Fig. 4D1 and D2, No.28).

3.4. Comparing paleoclimates from quantitative reconstruction and model simulation

Compared to other climatic factors (Figs. S52—S56), we observed a strong correspondence in PWetQ between the quantitative reconstructions from plant fossils and model simulations, especially in regions where PWetQ exceeded 600 mm (Fig. 5). However, there are some exceptions, for example, the quantitatively reconstructed PWetQ for the late Eocene Jianchuan and Markam assemblages (Fig. 5B), as well as middle Miocene Shanwang assemblage (Fig. 5F), which exceeds simulation results. In contrast, for some Miocene—Pliocene fossil assemblages, reconstructed values are lower than those simulated by models.

Simulation results indicate that PWetQ varied in response to paleogeographical changes (Fig. 5). In the early Eocene, southeastern China experienced abundant precipitation (Fig. 5A),
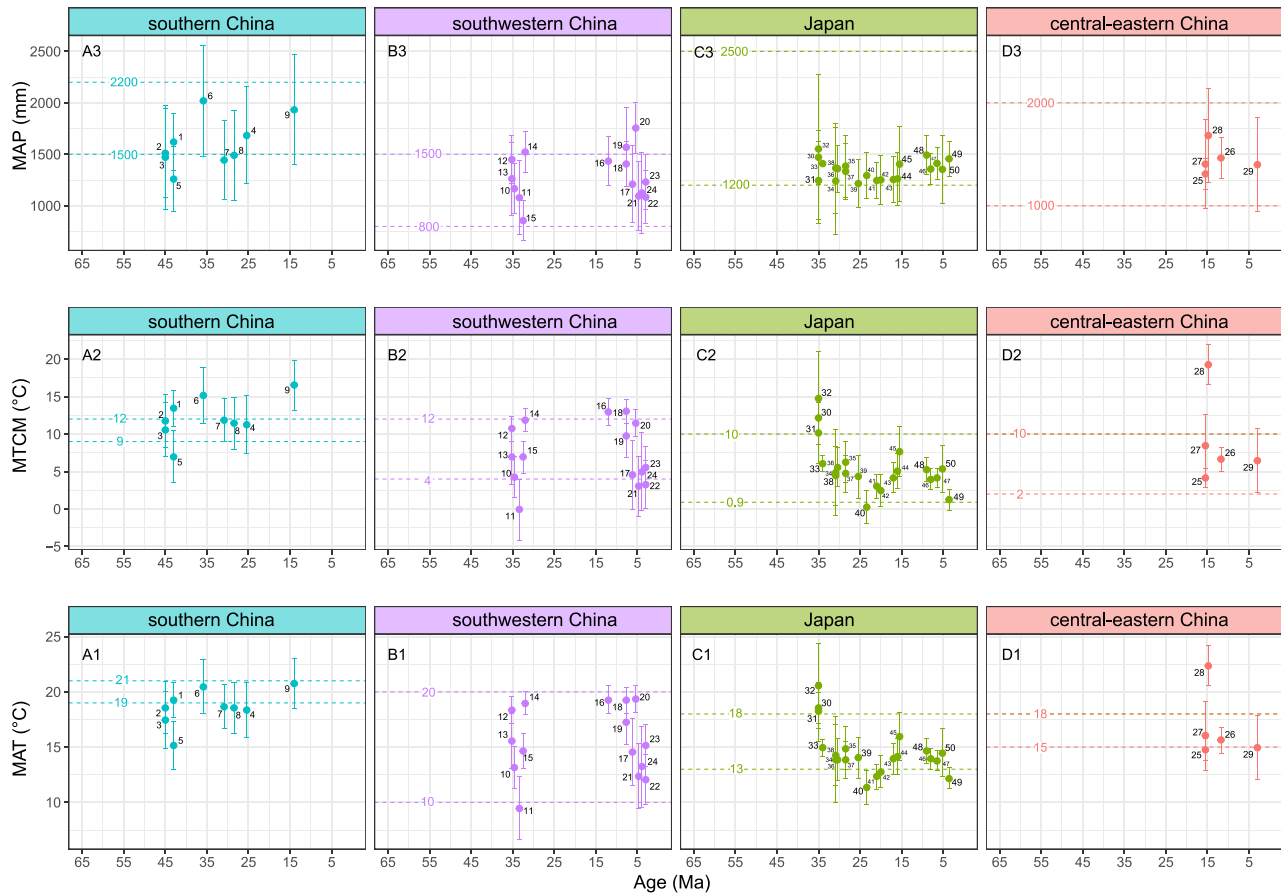
Fig. 4. The reconstructed paleoclimate (MAT, MTCM and MAP) for each fossil assemblages. The dashed lines showing climatic conditions of EBLFs for four regions.

whereas it became relatively dry in the late Eocene (Fig. 5B). During the Oligocene, precipitation in southwestern China gradually increased as a result of the continued uplift of the Tibetan Plateau, leading to a reduction in the central arid zone (Fig. 5C and D). Since the Miocene, southern China has generally witnessed increased precipitation, resulting in the disappearance of the arid zone (Fig. 5E—I).

4. Discussion

4.1. How to define EBLFs by plant fossils

One central question is how fossil plants can be used to identify historical occurrences of EBLFs. In this study, we use the components, paleoclimate, and paleovegetation of plant fossil assemblages to identify these historical occurrences of EBLFs.

EBLFs can be defined by the presence of EBLFs' components in fossil assemblages, e.g., Fagaceae, Lauraceae, Theaceae, and Magnoliaceae. These components are dominant in modern EBLFs and, therefore, serve as important indicators that identify this biome (Song, 2013; Song and Da, 2016). Over geological time, plant fossil assemblages exhibit distinct components and reflect various vegetation types. Some fossil assemblages (e.g., the late Eocene Jianchuan assemblage and the early Oligocene Wenshan assemblage in southwestern China, middle Eocene Changchang and Maoming assemblages in southern China, late Eocene Ube assemblage in Japan, late Miocne Tiantai flora in central-eastern China) represent evergreen broadleaved forests, of which Fagaceae and Lauraceae are the principal components, while Hamamelidaceae,

Fabaceae and other evergreen groups are also common (Huzioka and Takahasi, 1970; WGCPC, 1978; Li, 2010; Spicer et al., 2014, 2016; Aleksandrova et al., 2015; Herman et al., 2017; Huang, 2017). Some fossil assemblages (e.g., Pliocene Yongping, Lanping and Eryuan assemblages in southwestern China) represent evergreen sclerophyllous broad-leaved forests, with *Quercus* sect. *Heterobalanus* and conifers (*Pinus, Abies, Picea, Tsuga*) as the dominant elements (Tao and Kong, 1973; Huang et al., 2012, 2013, 2015, 2020; Su et al., 2013; Zhu et al., 2015, 2016). Some fossil assemblages (e.g., late Eocene Markam assemblage and early Oligocene Lühe assemblage in southwestern China, late Oligocene Noda assemblage in Japan and middle Miocene Shanwang assemblage in central-eastern China) represent evergreen-deciduous broadleaved mixed forests, dominated by the evergreen groups of Fagaceae, Magnoliaceae, Lauraceae and the deciduous groups of Betulaceae, Ulmaceae, Salicaceae (Hu and Chaney, 1940; Tanai and Uemura, 1991; Su et al., 2019; Deng et al., 2020; Wu et al., 2022b). Some fossil assemblages (e.g., early Oligocene Markam assemblage) represent alpine deciduous shrubs. Small-leaved shrubs such as *Salix, Rosa* and *Quercus* sect. *Heterobalanus* are main components (Su et al., 2019; Deng et al., 2020). Additionally, some fossil assemblages (e.g., middle Miocene Zhangpu assemblage and Guiping assemblage) represent tropical rainforests, dominated by tropical taxa including Annonaceae, Myrtaceae, and Burseraceae (Wang, 2018; Wang et al., 2021; Huang et al., 2021; Li et al., 2021b; Wu et al., 2021; Song et al., 2023).

Secondly, appropriate climatic conditions are essential for the emergence of EBLFs, as climate plays a key role in determining their geographic range. Our paleoclimatic analysis of plant fossils
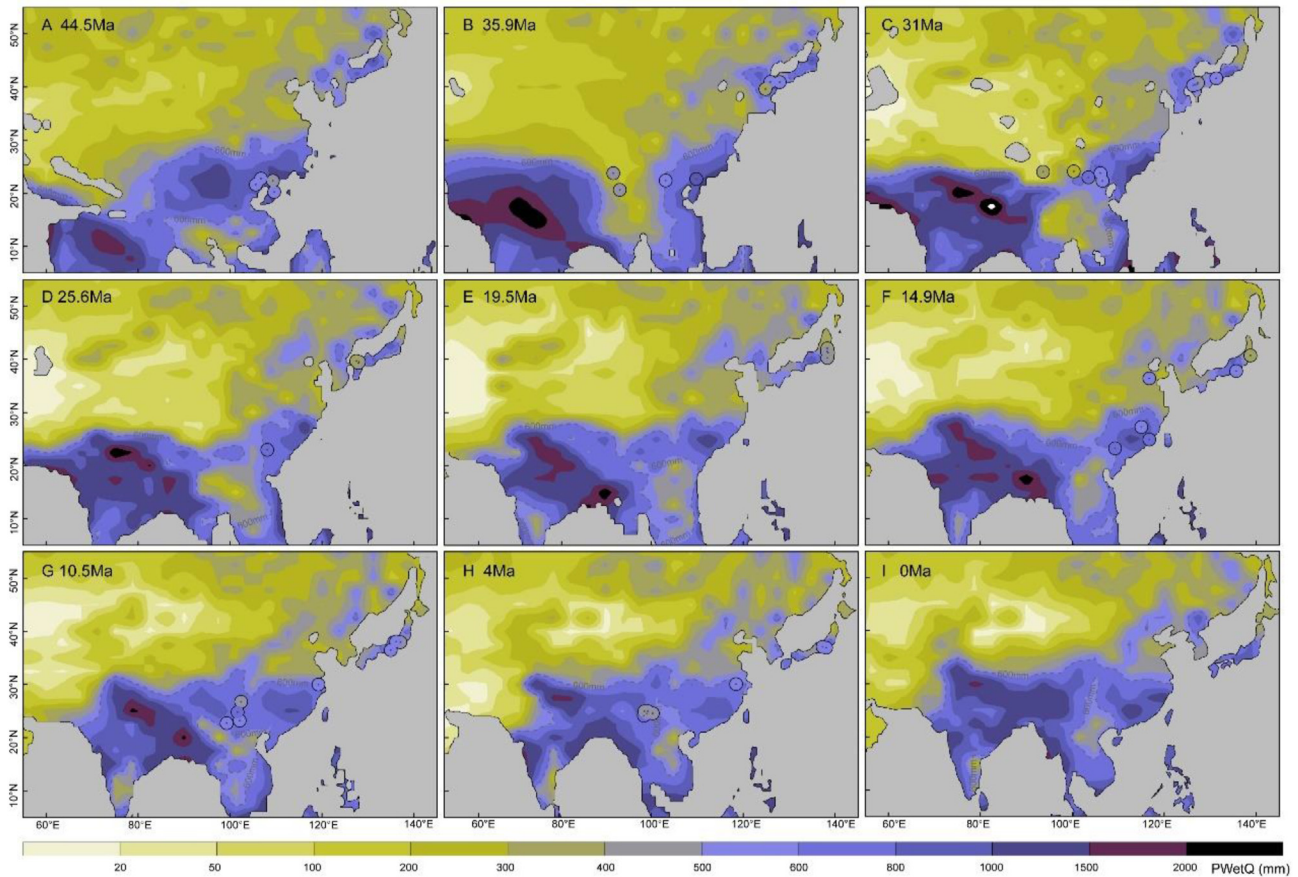
Fig. 5. Comparison of PWetQ (precipitation of the wettest quarter) between JPDFs (circles with dots) and numerical simulations. PWetQ equals to 600 mm is highlighted with grey contours.

indicates that most fossil assemblages are satisfactory for the emergence of EBLFs, although some are not (Fig. 4). The reconstructed MTCM is lower in the early Oligocene Markam assemblage than today. This may be due to the uplift of southeastern Xizang and a cooling trend during the early Oligocene, leading to an increase in deciduous components (Su et al., 2019; Deng et al., 2020). The MAT reconstructed for the early Miocene Shichiku assemblage falls below the minimum threshold because both the composition and foliar physiognomy of this assemblage resemble the Aniai-type flora. The Aniai-type flora is characterized by cool-temperate vegetation consisting of deciduous broad-leaved trees and conifers (Tanai, 1961; Yabe, 2008). The reconstructed temperatures of middle Miocene Zhangpu assemblage and Guiping assemblage exceed the maximum values on account of the Mid-Miocene Climatic Optimum (MMCO, ~14—17 million years ago), which resulted in a warmer climate leading to the presence of many tropical components in them (Wang, 2018; Wang et al., 2021; Huang et al., 2021; Li et al., 2021b; Wu et al., 2021; Song et al., 2023). In addition, the NLRs of some macrofossils were only identified at the genus or even family levels, which could potentially restrict the effectiveness of the method employed for climate reconstruction (Liu et al., 2011). This limitation may account for the lower reconstructed MAT of the middle Eocene Maoming assemblage. In comparison, we observed a high level of consistency between the quantitative reconstruction and simulated outputs in regions where PWetQ exceeds 600 mm (Fig. 5). This finding is also verified by the distribution of modern EBLFs and PWetQ in current observations (Fig. S1). Therefore, we deduce that PWetQ exceeding 600 mm is an important factor for the occurrence of EBLFs.

Thirdly, we can determine if a fossil assemblage represents an EBLF from its most similar extant forest vegetation. This is possible because modern vegetation in high-value grids can be regarded as the vegetation type most closely resembling that of the fossil assemblage. According to the distribution range of modern EBLFs (the white dashed lines in Fig. 1), regions with high similarity to most fossil assemblages predominantly coincide with the main areas of East Asian EBLFs today. Consequently, the paleovegetation of most fossil assemblages can be classified as EBLFs. In addition, the paleovegetation of a few fossil assemblages does not exhibit features of EBLFs due to their distinct composition. For example, the middle Miocene Shanwang and Guiping assemblages contain many tropical taxa, leading to a high similarity with areas located at lower latitudes in Southeast Asia. These areas are currently characterized by tropical monsoon forests or rainforests.

With a few exceptions (e.g., middle Miocene Shanwang and Guiping assemblages, early Oligocene Markam assemblage), the components, paleoclimate, and paleovegetation of plant fossil assemblages were able to identify EBLFs in East Asia during geological time.

4.2. Heterogeneous occurrence of evergreen broadleaved forests in East Asia

Combined with the peak period of appearance for EBLFs' dominant genera (Fig. 2), we inferred that occurrences of EBLFs show different temporal—spatial patterns. The earliest occurrence was in southern China during the middle Eocene (Fig. 6A), followed by southwestern China in the late Eocene—early Oligocene (Fig. 6B
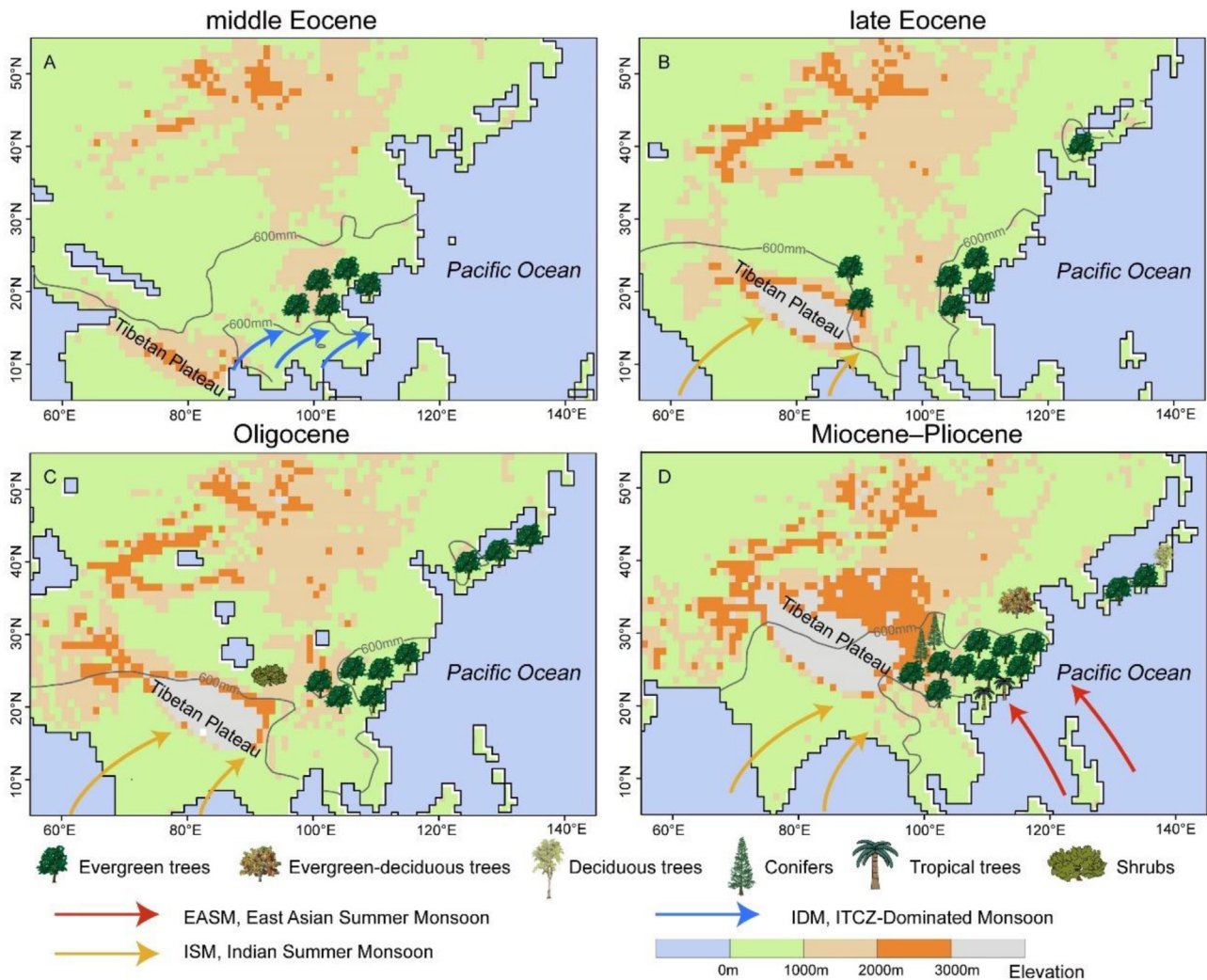
Fig. 6. Heterogeneous occurrence of EBLFs in East Asia during the Cenozoic. The land-sea boundary and topography were derived from the Scotese (2021). PWetQ equals to 600 mm is highlighted with grey contours.

and C), then Japan in the early Oligocene, and finally central-eastern China during the Miocene (Fig. 6C and D). Furthermore, our comparison of quantitative reconstruction and model simulation has led us to propose that PWetQ exceeding 600 mm may play a critical role in the occurrence of EBLFs (Fig. 6).

To some extent, our findings align with previous molecular dating studies (Xiang et al., 2016; Yu et al., 2017; Xiao et al., 2022; Qin et al., 2023; Zhang et al., 2024). Whether EBLFs originated in the Eocene, early Oligocene, or Oligocene−Miocene boundary, the paleobotanical evidence seems to support these estimates. However, evidence from molecular dating has primarily focused on the temporal emergence of EBLFs, overlooking their spatial distribution. The unique taphonomy of plant fossils allow for a direct exploration into the spatial occurrence of EBLFs in East Asia.

Moreover, when considering only paleobotanical evidence, our research indicates an earlier occurrence than previously thought, especially in southwestern China. This is due to the recent updates in the geological ages of the fossil assemblages collected in this region. This new chronological framework has advanced the occurrence time of EBLFs to the late Eocene−early Oligocene in southwestern China (Gourbet et al., 2017; Linnemann et al., 2018; Su et al., 2019; Tian et al., 2021).

4.3. The origin of evergreen broad-leaved forests in response to the evolution of the Asian Monsoon

The Asian Monsoon played a crucial role in the formation and development of EBLFs, which are especially impacted by precipitation (Song and Da, 2016; Yu et al., 2017; Li et al., 2021a; Ye and Li, 2022; Zhang et al., 2024). A recent review has demonstrated that the Asian Monsoon has undergone three phases of spatial expansion, indicating that EBLFs may have had a complex occurrence (Wu et al., 2022a).

The initiation of the Asian Monsoon is the tropical Asian Monsoon prevailing in southern Asia (the south of 20−22°N) before ~41 Ma, which was largely driven by the seasonal fluctuation of the Intertropical Convergence Zone (ITCZ) (Trenberth et al., 2000; Wang, 2009; Wang et al., 2014; Spicer et al., 2016; Farnsworth er al., 2019; Tardif et al., 2020). Previous studies have suggested that under the influence of tropical Asian Monsoon, the climate became humid and facilitated the appearance of EBLFs in southern China (Herman et al., 2017; Jin et al., 2017; Spicer, 2017). Palynological records across southern China have also observed a major environmental transition: from a relative high abundance of xerophilous taxa in the Paleocene−early Eocene to subtropical wet evergreen and deciduous broad-leaved mixed forest in middle

Eocene (Xie et al., 2019, 2020). Our study also demonstrates that EBLFs occurred in southern China during the middle Eocene, providing further evidence to support this hypothesis (Fig. 6A).

Subsequently, as a consequence of the full collision of India with Asia, fast northward movement of the southern margin of the Tibetan Plateau and Antarctic cooling, the Asian Monsoon expanded northward to the southern subtropical region (~26°N) ~41 Ma, synchronously promoting an abrupt dry–wet transitions and providing a unique opportunity for the emergence of EBLFs in southwestern China (Fig. 6B; Fang et al., 2021).

Finally, the modern-like pattern of the Asian Monsoon was fully established at ~26 Ma, probably driven by the uplift of the Tibetan Plateau and global climate change (Wu et al., 2022a). The ultimate establishment of the Asia Monsoon has shaped "a north-west dry and south-east humid" climate pattern in East Asia, which has been recognized as a major contributor to the formation of EBLFs in central-eastern China and Japan (Fig. 6C and D; Sun and Wang, 2005; Guo et al., 2008). Recent research has integrated modeling results and fossil data to demonstrate that the growth of north and northeastern Xizang altered the Asian monsoon system in the late Oligocene. This change led to a transition from deciduous broadleaf vegetation to evergreen broadleaf vegetation and increased plant diversity across southeastern Asia (Li et al., 2021a).

5. Conclusion

By intergrating the latest advances in paleobotany, our research has explored the occurrence of the EBLFs in East Asia from paleobotanical evidence. Different from the previously prevailing views in historical assembly of EBLFs, our findings highlight that the EBLFs in East Asia appeared in different temporal–spatial patterns: the earliest occurrence was in southern China in the middle Eocene, followed by southwestern China in the late Eocene–early Oligocene, Japan during the early Oligocene, and central-eastern China around the Miocene. In addition, we propose that PWetQ exceeding 600 mm is an important factor for the formation of EBLFs. Combined with the latest studies on the Asian monsoon, our findings suggest that the multistage evolution of Asian monsoon led to the diverse occurrence of EBLFs in East Asia.

CRediT authorship contribution statement

Jiagang Zhao: Writing – review & editing, Writing – original draft, Visualization, Formal analysis, Data curation. **Shufeng Li:** Writing – review & editing, Methodology, Formal analysis. **Jian Huang:** Visualization, Formal analysis. **Wenna Ding:** Visualization, Formal analysis. **Mengxiao Wu:** Writing – review & editing, Formal analysis. **Tao Su:** Writing – review & editing, Visualization. **Alexander Farnsworth:** Visualization, Methodology. **Paul J. Valdes:** Visualization, Methodology. **Linlin Chen:** Writing – review & editing, Visualization, Methodology. **Yaowu Xing:** Writing – review & editing, Writing – original draft, Visualization, Funding acquisition. **Zhekun Zhou:** Writing – review & editing, Writing – original draft, Funding acquisition, Conceptualization.

Declaration of competing interest

The authors declare no conflict of interests.

Acknowledgements

Appendix A. Supplementary data

Supplementary data to this article can be found online at https://doi.org/10.1016/j.pld.2024.07.004.

References

Aleksandrova, G.N., Kodrul, T.M., Jin, J.H., 2015. Palynological and paleobotanical investigations of Paleogene sections in the Maoming basin, South China. Stratigr. Geol. Correl. 23, 300–325.

Averianov, A., Obraztsova, E., Danilov, I., et al., 2017. Anthracotheriid artiodactyl anthracokeryx and an upper Eocene age for the Youganwo formation of southern China. Hist. Biol. 31, 1115–1122.

Azuma, H., García-Franco, J.G., Rico-Grey, V., et al., 2001. Molecular phylogeny of the Magnoliaceae: the biogeography of tropical and temperate disjunctions. Am. J. Bot. 88, 2275–2285.

BGMRYP (Bureau of Geology and Mineral Resources of Yunnan Province), 1990. Regional Geology of Yunnan Province. Geological Publishing House, Beijing, pp. 1–728 (in Chinese).

BGMRYP (Bureau of Geology and Mineral Resources of Yunnan Province), 1996. Lithostratigraphy of Yunnan Province. China University of Geosciences Press, Wuhan, pp. 211–309 (in Chinese).

Chen, X.H., Xiang, K.L., Lian, L., et al., 2020. Biogeographic diversification of Mahonia (Berberidaceae): implications for the origin and evolution of East Asian subtropical evergreen broadleaved forests. Mol. Phylogenet. Evol. 151, 106910.

Chen, Y.S., Deng, T., Zhou, Z., et al., 2018. Is the East Asian flora ancient or not? Natl. Sci. Rev. 5, 920–932.

Cox, P.M., 2001. Description of the TRIFFID Dynamic Global Vegetation Model. Tech rep. Met Office Hadley Centre, Exeter, UK.

Deng, M., Jiang, X.L., Hipp, A.L., et al., 2018. Phylogeny and biogeography of East Asian evergreen oaks (Quercus section Cyclobalanopsis; Fagaceae): insights into the Cenozoic history of evergreen broad-leaved forests in subtropical Asia. Mol. Phylogenet. Evol. 119, 170–181.

Deng, W.Y.D., Su, T., Wappler, T., et al., 2020. Sharp changes in plant diversity and plant-herbivore interactions during the Eocene–Oligocene transition on the southeastern Qinghai-Tibetan Plateau. Global Planet. Change 194, 103293.

Dong, S.S., Wang, Y.L., Xia, N.H., et al., 2021. Plastid and nuclear phylogenomic incongruences and biogeographic implications of Magnolia s.l. (Magnoliaceae). J. Syst. Evol. 60, 1–15.

Fang, J.Y., Guo, Z.D., Hu, H.F., et al., 2014. Forest biomass carbon sinks in East Asia, with special reference to the relative contributions of forest expansion and forest growth. Global Change Biol. 20, 2019–2030.

Fang, X.M., Yan, M.D., Zhang, W.L., et al., 2021. Paleogeography control of Indian monsoon intensification and expansion at 41 Ma. Sci. Bull. 66, 2320–2328.

Farnsworth, A., Lunt, D.J., Robinson, S.A., et al., 2019. Past East Asian monsoon evolution controlled by paleogeography, not CO₂. Sci. Adv. 5, eaax1697.

Fenton, I.S., Aze, T., Farnsworth, A., et al., 2023. Origination of the modern-style diversity gradient 15 million years ago. Nature 614, 708–712.

Foster, G.L., Royer, D.L., Lunt, D.J., 2017. Future climate forcing potentially without precedent in the last 420 million years. Nat. Commun. 8, 14845.

Gourbet, L., Leloup, P.H., Paquette, J.L., et al., 2017. Reappraisal of the Jianchuan Cenozoic basin stratigraphy and its implications on the SE Tibetan plateau evolution. Tectonophysics 700–701, 162–179.

Guo, Z.T., Sun, B., Zhang, Z.S., et al., 2008. A major reorganization of Asian climate by the early Miocene. Clim. Past 4, 153–174.

Hai, L., Li, X.Q., Zhang, J.B., et al., 2022. Assembly dynamics of East Asian subtropical evergreen broadleaved forests: new insights from the dominant Fagaceae trees. J. Integr. Plant Biol. 64, 2126–2134.

Herman, A.B., Spicer, R.A., Aleksandrova, G.N., et al., 2017. Eocene—early Oligocene climate and vegetation change in southern China: evidence from the Maoming Basin. Paleogeogr. Paleoclimatol. Paleoecol. 479, 126—137.

Hipp, A.L., Manos, P.S., Hahn, M., et al., 2020. Genomic landscape of the global oak phylogeny. New Phytol. 226, 1198—1212.

Hu, H.H., Chaney, R.W., 1940. Miocene Flora from Shantung Province, China. Carnegie Institution of Washington Publication, Washington D.C.

Huang, J., 2017. The Middle Miocene Wenshan Flora, Yunnan, Southwestern China and its Palaeoenvironment Reconstruction. PhD Thesis. Xishuangbannna Tropical Botanical Garden, Chinese Academy of Sciences.

Huang, J., Shi, G.L., Su, T., et al., 2017. Miocene exbucklandia (Hamamelidaceae) from Yunnan, China and its biogeographic and palaeoecologic implications. Rev. Palaeobot. Palynol. 244, 96—106.

Huang, J., Su, T., Jia, L.B., et al., 2018. A fossil fig from the Miocene of southwestern China: indication of persistent deep time karst vegetation. Rev. Palaeobot. Palynol. 258, 133—145.

Huang, J., Su, T., Lebereton-Anberree, J., et al., 2016b. The oldest *Mahonia* (Berberidaceae) fossil from East Asia and its biogeographic implications. J. Plant Res. 129, 209—223.

Huang, J.F., Li, L., van der Werff, H., et al., 2016a. Origins and evolution of cinnamon and camphor: a phylogenetic and historical biogeographical analysis of the *Cinnamomum* group (Lauraceae). Mol. Phylogenet. Evol. 96, 33—44.

Huang, L.L., Jin, J.H., Quan, C., et al., 2021. New occurrences of Altingiaceae fossil woods from the Miocene and upper Pleistocene of South China with phytogeographic implications. J. Palaegeogr. 10, 482—493.

Huang, Y.J., Jia, L.B., Su, T., et al., 2020. A warm-temperate forest of mixed coniferous type from the upper Pliocene Sanying Formation (southeastern edge of Tibetan Plateau) and its implications for palaeoecology and palaeoaltimetry. Paleogeogr. Paleoclimatol. Paleoecol. 538, 109486.

Huang, Y.J., Jacques, F.M.B., Liu, Y.S., et al., 2012. New fossil endocarps of *Sambucus* (Adoxaceae) from the upper Pliocene in SW China. Rev. Palaeobot. Palynol. 171, 152—163.

Huang, Y.J., Jacques, F.M.B., Liu, Y.S., et al., 2015. *Rubus* (Rosaceae) diversity in the late Pliocene of Yunnan, southwestern China. Geobios 48, 439—448.

Huang, Y.J., Liu, Y.S., Jacques, F.M.B., et al., 2013. First discovery of *Cucubalus* (Caryophyllaceae) fossil, and its biogeographical and ecological implications. Rev. Palaeobot. Palynol. 190, 41—47.

Huzioka, K., Takahasi, E., 1970. The Eocene flora of the Ube coal-field, southwest Honshu, Japan. J. Min. Coll. Akita Univ. - Ser. A Min. Geol. 4, 1—88.

Jin, J.H., Herman, A.B., Spicer, R.A., et al., 2017. Palaeoclimate background of the diverse Eocene floras of South China. Sci. Bull. 62, 1501—1503.

Karger, D.N., Conrad, O., Böhner, J., et al., 2017. Climatologies at high resolution for the earth's land surface areas. Sci. Data 4, 1—20.

Kunzmann, L., Li, S.F., Huang, J., et al., 2022. Assessment of phytogeographic reference regions for Cenozoic vegetation: a case study on the Miocene flora of Wiesa (Germany). Fossil Imprint 78, 1—43.

Li, X.C., 2010. The Late Cenozoic floras from eastern Zhejiang Province and their paleoclimatic reconstruction. PhD Thesis. Lanzhou University.

Li, L., Li, J., Rohwer, J.G., et al., 2011. Molecular phylogenetic analysis of the *Persea* group (Lauraceae) and its biogeographic implications on the evolution of tropical and subtropical Amphi-Pacific disjunctions. Am. J. Bot. 98, 1520—1536.

Li, Q.J., Utescher, T., Liu, Y.C., et al., 2022. Monsoonal climate of East Asia in Eocene times inferred from an analysis of plant functional types. Paleogeogr. Paleoclimatol. Paleoecol. 601, 111138.

Li, S.F., Mao, L.M., Spicer, R.A., et al., 2015. Late Miocene vegetation dynamics under monsoonal climate in southwestern China. Paleogeogr. Paleoclimatol. Paleoecol. 425, 14—40.

Li, S.F., Valdes, P.J., Farnsworth, A., et al., 2021a. Orographic evolution of northern Tibet shaped vegetation and plant diversity in eastern Asia. Sci. Adv. 7, eabc7741.

Li, Y.F., Huang, L.L., Quan, C., Jin, J.H., 2021b. Fossil wood of *Syzygium* from the Miocene of Guangxi, South China: the earliest fossil evidence of the genus in eastern Asia. IAWA J. 42, 435—441.

Lin, X.B., Wyrwoll, K.H., Chen, H.L., et al., 2015. An active east Asian monsoon at the Oligocene-Miocene boundary: evidence from the Sikouzi Section, Northern China. J. Geol. 123, 355—367.

Linnemann, U., Su, T., Kunzmann, L., et al., 2018. New U-Pb dates show a Paleogene origin for the modern Asian biodiversity hot spots. Geology 46, 3—6.

Liu, Y.S.C., Utescher, T., Zhou, Z.K., et al., 2011. The evolution of Miocene climates in North China: preliminary results of quantitative reconstructions from plant fossil records. Paleogeogr. Paleoclimatol. Paleoecol. 304, 308—317.

Lu, L.M., Mao, L.F., Yang, T., et al., 2018. Evolutionary history of the angiosperm flora of China. Nature 554, 234—238.

Nie, Z.L., Wen, J., Azuma, H., et al., 2008. Phylogenetic and biogeographic complexity of Magnoliaceae in the Northern Hemisphere inferred from three nuclear data sets. Mol. Phylogenet. Evol. 48, 1027—1040.

Palazzesi, L., Barreda, V.D., Cuitiño, J.I., et al., 2014. Fossil pollen records indicate that Patagonian desertification was not solely a consequence of Andean uplift. Nat. Commun. 5, 1—8.

Pan, Y., Birdsey, R.A., Fang, J.Y., et al., 2011. A large and persistent carbon sink in the world's forests. Science 333, 988—993.

Piao, S.L., Fang, J.Y., Ciais, P., et al., 2009. The carbon balance of terrestrial ecosystems in China. Nature 458, 1009—1013.

Qin, S.Y., Zuo, Z.Y., Guo, C., et al., 2023. Phylogenomic insights into the origin and evolutionary history of evergreen broadleaved forests in East Asia under Cenozoic climate change. Mol. Ecol. 32, 2850—2868.

Quan, C., Liu, Z.H., Utescher, T., et al., 2014. Revisiting the Paleogene climate pattern of East Asia: a synthetic review. Earth Sci. Rev. 139, 213—230.

Rao Mide, R.M., Steinbauer, M.J., Xiang, X.G., et al., 2018. Environmental and evolutionary drivers of diversity patterns in the tea family (Theaceae s.s.) across China. Ecol. Evol. 8, 11663—11676.

Scotese, C.R., 2021. An atlas of Phanerozoic paleogeographic maps: the seas come in and the seas go out. Annu. Rev. Earth Planet Sci. 49, 679—728.

Song, H.Z., Huang, L.L., Xiang, H.L.L., et al., 2023. First reliable Miocene fossil winged fruits record of *Engelhardia* in Asia through anatomical investigation. iScience 26, 106867.

Song, Y.C., Da, L.J., 2016. Evergreen broad-leaved forest of East Asia. In: Box, E.O. (Ed.), Vegetation Structure Andfunction at Multiple Spatial, Temporalandconceptual Scales. Springer International, Switzerland, pp. 101—128.

Song, Y.C., 2013. Evergreen Broad-Leaved Forests in China: Classification, Ecology, Conservation. Higher Education Press, Beijing, China.

Spicer, R.A., 2017. Tibet, the Himalaya, Asian monsoons and biodiversity—In what ways are they related? Plant Divers 39, 233—244.

Spicer, R.A., Herman, A.B., Liao, W.B., et al., 2014. Cool tropics in the middle Eocene: evidence from the Changchang flora, Hainan Island, China. Paleogeogr. Paleoclimatol. Paleoecol. 412, 1—16.

Spicer, R.A., Yang, J., Herman, A.B., et al., 2016. Asian Eocene monsoons as revealed by leaf architectural signatures. Earth Planet Sci. Lett. 449, 61—68.

Su, T., Jacques, F.M.B., Spicer, R.A., et al., 2013. Post-Pliocene establishment of the present monsoonal climate in SW China: evidence from the late Pliocene Longmen megaflora. Clim. Past 9, 1911—1920.

Su, T., Spicer, R.A., Li, S.H., et al., 2019. Uplift, climate and biotic changes at the Eocene—Oligocene transition in south-eastern Tibet. Natl. Sci. Rev. 6, 495—504.

Sun, X.J., Wang, P.X., 2005. How old is the Asian monsoon system?—palaeobotanical records from China. Paleogeogr. Paleoclimatol. Paleoecol. 222, 181—222.

Tanai, T., 1961. Neogene floral change in Japan. Journal of the Faculty Science, Hokkaido University, Series IV (11), 119—398 pls.1—32.

Tanai, T., Uemura, K., 1991. The Oligocene Noda Flora from the Yuyawan area of the western end of Honshu, Japan. Part 2. Bull. Natn. Sci. Mus. Ser. C. 17, 81—90.

Tang, C.Q., 2015. Evergreen broad-leaved forests. In: Tang, C.Q. (Ed.), The Subtropical Vegetation of Southwestern China: Plant Distribution, Diversity and Ecology. Springer, Utrecht, pp. 60—105.

Tao, J.R., Kong, Z.C., 1973. The fossil florule and sporo-pollen assemblage of Shang-in coal series of Eryuan, Yunnan. Acta Bot. Sin. 15, 120—126.

Tardif, D., Fluteau, F., Donnadieu, Y., et al., 2020. The origin of Asian monsoons: a modelling perspective. Clim. Past 16, 847—865.

Tian, Y.M., Spicer, R.A., Huang, J., et al., 2021. New early Oligocene zircon U-Pb dates for the 'Miocene' Wenshan basin, Yunnan, China: biodiversity and paleoenvironment. Earth Planet Sci. Lett. 565, 116292.

Trenberth, K.E., Stepaniak, D.P., Caron, J.M., 2000. The global monsoon as seen through the divergent atmospheric circulation. J. Clim. 13, 3969—3993.

Utescher, T., Bruch, A.A., Erdei, B., et al., 2014. The Coexistence Approach—theoretical background and practical considerations of using plant fossils for climate quantification. Paleogeogr. Paleoclimatol. Paleoecol. 410, 58—73.

Valdes, P.J., Armstrong, E., Badger, M.P., et al., 2017. The BRIDGE HadCM3 family of climate models: HadCM3@ Bristol v1. 0. Geosci. Model Dev. (GMD) 10, 3715—3743.

Valdes, P.J., Scotese, C.R., Lunt, D.J., 2021. Deep ocean temperatures through time. Clim. Past 17, 1483—1506.

Wang, B., Shi, G., Xu, C., et al., 2021. The mid-Miocene Zhangpu biota reveals an outstandingly rich rainforest biome in East Asia. Sci. Adv. 7, eabg0625.

Wang, P.X., 2009. Global monsoon in a geological perspective. Chin. Sci. Bull. 54, 1113—1136.

Wang, P.X., Wang, B., Cheng, H., et al., 2014. The global monsoon across timescales: coherent variability of regional monsoons. Clim. Past 10, 2007—2052.

Wang, Q., Spicer, R.A., Yang, J., et al., 2013. The Eocene climate of China, the early elevation of the Tibetan Plateau and the onset of the Asian Monsoon. Glob. Chang. Biol. 19, 3709—3728.

Wang, Z.X., 2018. Fossil Plants with Microstructures from the Miocene of Zhangzhou, Fujian and Palaeoclimatic Reconstructions. PhD Thesis. Lanzhou University.

West, C.K., Greenwood, D.R., Reichgelt, T., et al., 2020. Paleobotanical proxies for early Eocene climates and ecosystems in northern North America from middle to high latitudes. Clim. Past 16, 1387—1410.

Writing Group of Cenozoic Plant of China (WGCPC), 1978. Fossil Plants of China. Vol. 3: Cenozoic Plants from China (in Chinese). Science Press, Beijing.

Willard, D.A., Donders, T.H., Reichgelt, T., et al., 2019. Arctic vegetation, temperature, and hydrology during Early Eocene transient global warming events. Global Planet. Change 178, 139—152.

Wu, C.Y., 1995. Vegetation of China. Science Press, Beijing.

Wu, F.L., Fang, X.M., Yang, Y.B., 2022a. Reorganization of Asian climate in relation to Tibetan Plateau uplift. Nat. Rev. Earth Environ. 3, 684—700.

Wu, M.X., Huang, J., Spicer, R.A., et al., 2022b. The early Oligocene establishment of modern topography and plant diversity on the southeastern margin of the Tibetan Plateau. Global Planet. Change 214, 103856.

Wu, X.K., Zhang, H., Kodrul, T.M., et al., 2021. First fossil *Fokienia* (Cupressaceae) in South China and its palaeogeographic and palaeoecological implications. Front. Earth Sci. 9, 709663.

Xiang, X.G., Mi, X.C., Zhou, H.L., et al., 2016. Biogeographical diversification of mainland Asian *Dendrobium* (Orchidaceae) and its implications for the historical dynamics of evergreen broadleaved forests. J. Biogeogr. 43, 1310–1323.

Xiang, X.G., Wang, W., Li, R.Q., et al., 2014. Large-scale phylogenetic analyses reveal fagalean diversification promoted by the interplay of diaspores and environments in the Paleogene. Perspect. Plant Ecol. Evol. Syst. 16, 101–110.

Xiao, T.W., Yan, H.F., Ge, X.J., 2022. Plastid phylogenomics of tribe Perseeae (Lauraceae) yields insights into the evolution of East Asian subtropical evergreen broad-leaved forests. BMC Plant Biol. 22, 1–15.

Xie, Y.L., Wu, F.L., Fang, X.M., 2019. Middle Eocene East Asian monsoon prevalence over southern China: evidence from palynological records. Global Planet. Change 175, 13–26.

Xie, Y.L., Wu, F.L., Fang, X.M., 2020. A major environmental shift by the middle Eocene in southern China: evidence from palynological records. Rev. Palaeobot. Palynol. 278, 104226.

Xing, Y.W., Onstein, R.E., Carter, R.J., et al., 2014. Fossils and a large molecular phylogeny show that the evolution of species richness, generic diversity, and turnover rates are disconnected. Evolution 68, 2821–2832.

Xu, J.X., Ferguson, D.K., Li, C.S., et al., 2008. Late Miocene vegetation and climate of the Lühe region in Yunnan, southwestern China. Rev. Palaeobot. Palynol. 148, 36–59.

Yabe, A., 2008. Early Miocene terrestrial climate inferred from plant megafossil assemblages of the Joban and Soma areas, Northeast Honshu, Japan. Bull. Geol. Surv. Japan 59, 397–413.

Yan, Y.J., Davis, C.C., Dimitrov, D., et al., 2021. Phytogeographic history of the tea family inferred through high-resolution phylogeny and fossils. Syst. Biol. 70, 1256–1271.

Ye, J.W., Li, D.Z., 2022. Diversification of East Asian subtropical evergreen broad-leaved forests over the last 8 million years. Ecol. Evol. 12, e9451.

Yu, X.Q., Gao, L.M., Soltis, D.E., et al., 2017. Insights into the historical assembly of East Asian subtropical evergreen broadleaved forests revealed by the temporal history of the tea family. New Phytol. 215, 1235–1248.

Zhang, Q., Yang, Y.C., Liu, B., et al., 2024. Meta-analysis provides insights into the origin and evolution of East Asian evergreen broad-leaved forests. New Phytol. 242, 2369–2379.

Zhang, Q., Zhao, L., Folk, R.A., et al., 2022. Phylotranscriptomics of Theaceae: generic level relationships, reticulation and whole genome duplication. Ann. Bot. 129, 457–471.

Zhu, H., Huang, Y.J., Ji, X.P., et al., 2016. Continuous existence of *Zanthoxylum* (Rutaceae) in southwest China since the Miocene. Quat. Int. 392, 224–232.

Zhu, H., Jacques, F.M.B., Wang, L., et al., 2015. Fossil endocarps of *Aralia* (Araliaceae) from the upper Pliocene of Yunnan in southwest China, and their biogeographical implications. Rev. Palaeobot. Palynol. 223, 94–103.